COMPUTER-AIDED CIVIL AND INFRASTRUCTURE ENGINEERING

Computer-Aided Civil and Infrastructure Engineering **29** (2014) 416–432

Localized Structural Damage Detection: A Change Point Analysis

M. B. Nigro, S. N. Pakzad* & S. Dorvash

Department of Civil and Environmental Engineering, Lehigh University, Bethlehem, PA 18015, USA

Abstract: *Many current damage detection techniques rely on the skill and experience of a trained inspector and also require a priori knowledge about the structure's properties. However, this study presents adaptation of several change point analysis techniques for their performance in civil engineering damage detection. Literature shows different statistical approaches which are developed for detection of changes in observations for different applications including structural damage detection. However, despite their importance in damage detection, control charts and statistical frameworks are not properly utilized in this area. On the other hand, most of the existing change point analysis techniques were originally developed for applications in the stock market or industrial engineering processes; utilizing them in structural damage detection needs adjustments and verification. Therefore, in this article several change point detection methods are evaluated and adjusted for a damage detection scheme. The effectiveness of features from a statistics based local damage detection algorithm called Influenced Coefficient Based Damage Detection Algorithm (IDDA) is expanded for a more complex structural system. The statistics used in this study include the univariate Cumulative Sum, Exponentially Weighted Moving Average (EWMA), Mean Square Error (MSE), and multivariate Mahalanobis distances, and Fisher Criterion. They are used to make control charts that detect and localize the damage by correlating locations of a sensor network with the damage features. A Modified MSE statistic, called ModMSE statistic, is introduced to remove the sensitivity of the MSE statistic to the variance of a data set. The effectiveness of each statistic is analyzed.*

1 INTRODUCTION

Structural health monitoring (SHM) research has become a vital tool in maintaining the integrity of structures that has been refined over the years. Damage detection is a fundamental element of SHM practice and is one of the most challenging research tasks for the civil engineering community. Literature shows numerous techniques for damage detection such as those in Khelifa and Guessasma (2013), O'Byrne et al. (2013), Osornio-Rios et al. (2012), which are classified in different ways. Some are traditional approaches such as nondestructive evaluation (NDE) techniques. Many of these rely on the skill and experience of a trained inspector and also require *a priori* knowledge about the structure's properties; on the other hand, some are data-driven techniques which rely on measurement and monitoring and can be classified into model-based and model-free methods (Dorvash et al., 2013). A class of data-driven approaches uses modal parameter identification with data in time and frequency domain (Yao and Pakzad, 2013) in which modal frequencies, mode shapes (West, 1984) or mode shape curvatures (Pandey and Biswas, 1995) are chosen as damage sensitive features (Doebling et al., 1998). Derivation of some of these parameters can be found in Sirca and Adeli (2012). Additionally, a review of these methods can be found in Salawu (1997) and Cruz and Salgado (2009). However, methods like these are only proper for detection of global damages in the structure and are generally unable to detect local damage (Alvandi and Cremona, 2006). These features are not sensitive enough to the changes in local elements of the structure hence they require high signal-to-noise ratio of the measurement data as well as moderate damage levels (Farrar et al., 1994).

As an answer to the shortcomings of these damage detection techniques, model-free approaches can be utilized. Xu and Humar (2006), Philips and Wu (2011), Talebinejad et al. (2011), and Fugate et al. (2001) have used such vibration techniques. These techniques can be utilized through the implementation of localized sensor networks as used in Hu et al. (2013), Nishikawa et al. (2012), Luo et al. (2013), Glisic et al. (2013), and Walsh et al. (2013).

*To whom correspondence should be addressed. E-mail: *pakzad@lehigh.edu.*

DOI: 10.1111/mice.12059

By utilizing different types of dense sensor networks, such as in Hampshire and Adeli (2000), output only algorithms can be developed in which there is no need for *a priori* knowledge of the structure's properties or suspected location of damage. Although these localized model-free approaches are easy to implement and effective in reflecting the changes in the structure's behavior, they are dependent on statistical analysis to determine the significance of the changes in the data. One type of statistical approach is the use of Bayesian probability frameworks such as that used by Yin et al. (2012). Umesha et al. (2009), Xiang (2012), Adeli and Jiang (2009), Jiang and Adeli (2007), Park et al. (2007), Jiang and Adeli (2008a), and Jiang and Adeli (2008b) use another type of framework creating a wavelet transformation. Yet another type of statistical approach is the use of control charts in which thresholds are used to distinguish between assignable and common changes in the data. This type of statistical approach is used in the scope of this article.

The contribution of this article is in establishing and comparing the effectiveness of five different control statistics in detecting damage for the application of SHM. Performance of different control statistics are evaluated through implementation on data obtained from laboratory frame model. Moreover, a modified Mean Square Error (MSE) statistic is introduced to eliminate the effects of variation within data sets. The performance of the developed statistic is also studied through the experiment discussed in this article. The article is organized as follows: Section 2 presents an introduction to change point detection in which the relevant literature is reviewed. Bootstrapping and its applications are presented along with a review of the five statistical change point analysis methods evaluated in this study. This section is followed by an introduction to the utilized damage indicators in Section 3. Section 4 introduces the test specimen and adapts the damage indicators for this specific structure. Results are shown in Section 5, along with the discussion and verification for using the modified MSE statistic. Conclusions will include a comparison of each statistic's performance and poses questions for future work to increase the accuracy of damage localization in Section 6.

2 AN INTRODUCTION TO CHANGE POINT ANALYSIS STATISTICS

Control statistics can be used to monitor a change in a process. However, there are two causes of variation that could occur in a process: common causes and assignable causes. For instance, in civil engineering, a structure's properties could have changed slightly with the passage of time (common causes) and is not damaged, or a structure could be damaged during an event (assignable cause). To distinguish between the two, control charts can be used to provide boundary limits for a change in a process. Once the boundary is crossed, the change in the process can be denoted as out of control from an assignable cause and, in the case of civil engineering, a structure can be deemed damaged.

Literature presents several different types of control statistics that can be used for change point detection in different processes. As an early effort in this area, the standard univariate Shewhart $\bar{X}$ control chart was introduced in 1924 by Walter Shewhart. Since then, control schemes have found widespread application in different disciplines including civil engineering. For example Sohn et al. (2000) applied Shewhart control charts to successfully detect the irregularities associated with damaged structures. Other control statistics have since been introduced. For instance, the Cumulative Sum (CUSUM) indicator, a statistical method that can be performed on different types of data, was used by Taylor (2011) and advanced by Hawkins (1981). Another control statistic first introduced by Roberts (1959) is called the Exponentially Weighted Moving Average (EWMA). Lucas and Saccuci (1990) as well as Macgregor and Harris (1990) have used this statistic.

Challenges in univariate quality control occur when one observes a set of quality characteristics that have components with the potential to be interrelated. One major flaw in using the mentioned univariate control statistics is that they can only monitor one variable at a time. It is common in civil engineering that more than one variable would need to be examined. Although it could be argued that univariate control charts could be applied independently to each component of the multivariate data, misleading results may be obtained in some cases due to failure to allow for the inherent relationship among the components of the multivariate data (Zamba and Hawkins, 2006). Therefore, this article also explores multivariate control statistics. The original and best known work in multivariate control charts are those described in Hotelling (1947), using the T^2 statistic. This statistic is a direct multivariate equivalent to the Shewart $\bar{X}$ control statistic and is used to create Mahalanobis distances which extract damage features by measuring the amount of variation from a reference condition. Zamba and Hawkins (2006) use these distances in their work along with Wang and Ong (2008), Pompe and Feelders (1997), and Gul and Catbas (2009). To alleviate the need for initiating assumptions, Verdier and Ferreira (2011) propose another distance that is nonparametric. This new distance can be applied without the postulation of normal probability distribution. Mosavi et al. (2011) introduced another statistic, the

Fisher Criterion, to measure the significance of the magnitude of the Mahalanobis distance.

This study aims to provide a better understanding of the performance of different change point detection methods in civil engineering damage detection through implementation and validation of five different approaches. The comparison of the CUSUM, MSE, and EWMA charts is unified by using bootstrapping to create the threshold for each method. This way, these common and widely used statistics can be evaluated under the same threshold type. Additionally, for multivariate methods, Mahalanobis distances and Fisher Criterion damaged detection methods are chosen as a focus because they use the T^2 statistic, the most direct equivalent to the original and trusted univariate statistic, the $\bar{X}$ statistic.

2.1 Univariate change point detection approaches and their enhancements

2.1.1 EWMA. The EWMA statistic (Z) is especially effective in detecting "small persistent process shifts" (Steiner, 1999). It is an exponentially weighted average of all previous observations in a vector of length n shown in Equation (1):

$$Z_i = \lambda Y_{i+1} + (1-\lambda) Z_{i-1} \quad 0 < \lambda < 1 \tag{1}$$

where Y_i are components of the data set and typical values of λ are between 0.05 and 0.25 for quality monitoring techniques. It should be noted that $Z_0 = \lambda Y_1$ and i continues until $n - 1$. The control limits that are prederived for this statistic from Lucas and Saccuci (1990) are based on the asymptotic standard deviation of the control statistics and defined as three standard deviations away from the mean of the statistic. This value of three correlates to the point in a standard normal distribution plot (of mean zero and standard deviation of one) in which 99.7% of the area under the curve is included. It will be shown in Section 5.1 that this control limit does not suit all data. Therefore, bootstrapping will be used for comparison of the EWMA statistic with the rest of the control statistics discussed.

2.1.2 CUSUM. The CUSUM statistic is one approach which is commonly used for detecting change points in data sets. It is a very flexible method which can be applied to different types of data (Lucas and Saccuci, 1990). The cumulative sums $S_0, S_1, S_2 \ldots S_n$ can be calculated by the following equations where $X_1, X_2 \ldots X_n$ are the components of the data set (Taylor, 2011).

$$S_0 = 0 \tag{2}$$

$$S_i = S_{i-1} + (X_i - \overline{X_i}) \tag{3}$$

where, $\bar{X}_1$ is the mean of all the known in control data. Shown in Equation (3), the cumulative sums are not simply sums, but the sums of the differences between the values of data and the average of the data. In a damage detection scheme, a drastic change in the slope, or inflection point, indicates a possible damaged state of the structure. In the case where two segments of data are considered from a pre- and post damaging event, there should only be one change point in the data: when the data switches from an undamaged set to a damaged set. This change point would occur where the magnitude of the CUSUM chart was furthest away from zero and is called the CUSUM Indicator. This indicator can then be investigated by comparing it to threshold conditions to verify the state of the structure.

2.1.3 MSE Indicator. The MSE Indicator is calculated from a scheme that splits the data into two segments, from 1 to m and $m + 1$ to n ($1 \leq m \leq n - 1$). The data is then analyzed to see how well it fits the two estimated averages of those segments (Taylor, 2011). The point after the value that minimizes MSE indicates a possible change point in the data. MSE can be defined as

$$\text{MSE}\, m = \sum_{i=1}^{m} (X_i - X_1)^2 + \sum_{i=m=1}^{n} (X_i - X_2)^2 \tag{4}$$

$$X_1 = \frac{\sum_{i=1}^{m} X_i m}{m} \text{ and } X_2 = \frac{\sum_{i=m+1}^{n} X_i}{n-m} \tag{5}$$

where X_i is a member of the data set and X_1 and X_2 are the means of the two segments of the data. The MSE is dependent on the variability within the data. Consequently, the statistic must be modified to expunge the variance between the two data segments produced while still maintaining their independent means. Therefore, a new statistic, Modified MSE (ModMSE) is introduced as

$$\text{ModMSE}\,(m) = \sum_{i=2}^{m} \left(\frac{X_i - X_1}{\text{std}(X_{k|k=2\ldots i})} \right)^2 + \sum_{i=m+1}^{n} \left(\frac{X_i - X_2}{\text{std}(X_{k|k=m+1\ldots i})} \right)^2 \tag{6}$$

where variables are defined the same as in Equation (5); however, the value is normalized by the variance (i.e., std $[X_k]^2$) of the two independent vectors. Results for the verification of this statistic are shown in Section 5.3. It is noted the statistic starts at the second value in the vector to avoid using the standard deviation of a single number which would produce numerical instability.

2.1.4 Bootstrapping for threshold construction. Bootstrapping is used to create a threshold for the three

univariate control statistics discussed above. It creates multiple iterations of new data generated by randomly resampling the original data with replacement. Because these new data vectors are randomly sampled, the properties of the statistic they create will have similar properties to an undamaged data set and therefore can be used as a basis for comparison. Once a statistic crosses the threshold bounds produced by the bootstrap, the change in the data can be deemed from an assignable cause and the properties of the system have changed significantly to become out of control. In damage detection schemes, this means damage has occurred.

A bootstrap is only as good as its confidence level defined in Equation (7):

$$\frac{X}{N} = \frac{\#\text{ of Ranges for } S_{\text{diffzero}} < S_{\text{diff}}}{\#\text{ of total Bootstrap samples performed}} \tag{7}$$

In this equation S_{diffzero} is the difference between the maximum and minimum value of each bootstrapped data set, S_{diff} is the range of the original data, N is the number of bootstrap samples performed, and X the number of bootstraps for which S_{diffzero} was less than the original S_{diff} of the data.

2.2 Multivariate change point detection approaches

2.2.1 Mahalanobis distance using the T^2 statistic. When significant changes in more than one variable are to be identified, multivariable models are applicable. As a measure for quantification of changes, assume that there is a matrix of damage indices associated with a certain condition and a certain location on the structure. The Mahalanobis distance gives the distance between selected damage features corresponding to a condition of interest and those corresponding to a reference condition. The Mahalanobis distance $D_m(x)$ can be computed by using Equation (8) from Mosavi et al. (2011)

$$D_m(x) = \sqrt{(x-\mu)^T S^{-1}(x-\mu)} \tag{8}$$

where μ is the mean of the damage feature x, and S is the covariance. In detection schemes, a larger Mahalanobis distance indicates that the location is closer to damage.

2.2.2 Fisher Criterion. Although a Mahalanobis distance, $D_m(x)$, reflects the changes in a set of damage indices, a criterion is needed to statistically investigate the significance of this change. To address this need, the Fisher Criterion can be utilized (Mosavi et al., 2011). The Fisher Criterion measures the actual deviation of Mahalanobis distance under the damage condition of interest versus those for the healthy condition. This criterion, f, can be obtained using Equation (9)

$$f = \frac{(m_{\text{D}} - m_{\text{H}})^2}{\sigma_{\text{D}}^2 + \sigma_{\text{H}}^2} \tag{9}$$

where m_{D} and m_{H} correspond to the mean values of the Mahalanobis distances for healthy and damaged conditions, and σ_{D} and σ_{H} represent the standard deviations of those vectors, respectively. The larger the statistic, the more likely the process is out of control. A threshold value of $T = \mu + 1.96\sigma$ is used. Here, μ and σ are the mean value and standard deviation of the Fisher Criterion statistic from all of the locations on the structure. This threshold is chosen because 97.5% of the area under a normal curve lies within 1.96 standard deviations of the mean (Mosavi et al., 2011).

3 LOCALIZED DAMAGE DETECTION METHOD

The damage features studied in this article are linear regression coefficients produced by an algorithm called Influenced Coefficient Based Damage Detection Algorithm (IDDA) developed and tested in Dorvash et al. (2010, 2013) on a prototype lab specimen. The key to structural damage diagnosis is to extract features of the structural response that present a unique pattern to the state of the structure using a single or limited number of input/output signals (Qiao et al., 2012). In this algorithm the response of the structure is monitored at various locations and coefficients of correlations between different responses are extracted. When the damage occurs, the relationship between responses changes, which will be reflected in the influence coefficients and indicate the existence of damage. Additionally, the location of damage can be identified by considering the location of the sensors associated with the changing coefficients. The mathematical model which represents the physical system for this damage detection algorithm is briefly presented in this section.

The relationship between responses at different locations of a structure can be established using an Auto Regressive with Exogenous term (ARX) model as follows:

$$\sum_{p=0}^{P} a_p y(n-p) = \sum_{q=1}^{Q} b_q x(n-q) + \varepsilon(n) \tag{10}$$

Here y and x are the outputs of a structure's response to excitation, a_p and b_q's are ARX coefficients, $\varepsilon(n)$ represents the residuals, n is the time index, and P and Q are orders of the autoregressive and exogenous parts of the ARX model, respectively. Based on this mathematical representation, the response at different time steps can be estimated having the past and current outputs. These

damage features are similar to those found in literature. Sohn et al. (2001) and Yao and Pakzad (2010) also use a similar Auto Regressive (AR) and ARX model for feature extraction and pattern recognition. Similarly, Qioa and Esmaeily (2011) use an ARX regression model for time-history damage features. This model will be used in the multivariate schemes in this article. The accuracy of this model is dependent on the selected model orders. Although higher model orders, in general, deliver more details of the system and reduce the estimation bias, it is always desired to keep the order at the minimum level to avoid over-parameterization. The model order is chosen using the Akaike Information Criterion explained in Section 4.3.

A special case for the assumed linear system is developed by assuming P and Q equal to zero:

$$y_j = \alpha y_i + \beta + \varepsilon \tag{11}$$

which correlates the response at node j to current response at node i. Because the effects of previous time steps are removed from the equation, the intercept (β) is added into Equation (11) to account for the initial conditions. This model, in which a single parameter, α, represents the damage index, is utilized to derive univariate influence coefficients used in the univariate control schemes.

4 TEST SETUP AND IMPLEMENTATION OF IDDA

4.1 Test specimen

A two-bay, steel tube frame testbed was constructed at the laboratory of Advanced Technology for Large Structural Systems (ATLSS) at Lehigh University for the implementation of the damage detection algorithm and the verification of the performance of different change point detection methods, as shown in Figure 1. To simulate damage, there are nine sections that can be changed throughout the frame.

These interchangeable sections are 0.19 m long and have different cross-sectional properties than the healthy state (shown in Table 1) which correspond to a 20% reduction in member moment of inertia (only for the length of the interchangeable piece). It is important to note that these property changes only correspond to less than a 0.5% decrease in the overall lateral stiffness of the frame when one piece is replaced at a time (the global lateral stiffness of the frame reduces by up to this amount due to simulated damage at different locations). This change in stiffness may be insignificant on the global scale but may have a larger impact on the response of the structure locally. A small change in stiffness can be from a small crack, corrosion, or any other damage mode representing a loss in cross-sectional area resulting in the loss of stiffness. Damage has been considered as such stiffness reduction in Farrar et al. (1999) and Nichols et al. (2003).

Fig. 1. Experimental structure. Also shown, an interchangeable piece.

To collect data, 21 wired accelerometers, labeled R, C, and L for the right, center, and left joint of the frame, were spaced evenly throughout the two-span frame as shown in Figure 2. Location of sensors are selected such that main connections of the frame are surrounded by clusters of sensors capturing their behavior (further studies are required to determine the optimized location of sensors to efficiently detect the onset of change in the behavior of the structure). The relatively dense arrangement of sensors is deemed practical in real-world implementations, considering the recent technological advancements which have resulted in development of affordable sensing systems (e.g., wireless sensor networks).

During testing, there were 20 runs taken from the undamaged state of the frame which serve as a baseline for comparison. In determining the number of test runs, there needed to be enough tests before the occurrence of damage to have a foundation for assessment. According to Tague (2004), only when there are at least 20 sequential points from a period when the process is in control, is the basis for comparison complete.

The damage case for this implementation consists of switching out the interchangeable section corresponding to the location of sensor R5. Switching out one interchangeable piece is the smallest amount of damage that can be simulated using this experimental structure. Therefore, the localization of damage of the different change point methods can be accurately assessed. The robustness of the algorithm can be tested as well to see how sensitive it is to such a small change. After this section was replaced with its damaged counterpart, an additional 20 tests were run. These tests will serve as the unknown state of the structure after a damaging event. For each run, the sampling rate was 500 Hz and 10,000 samples were recorded in a 20-second duration. Based on Finite Element analysis, the first three frequencies of the frame are 13.66, 21.95, and 31.58 Hz. These

Table 1
Geometry of baseline and interchangeable sections

Feature	*Baseline sections*	*Interchangeable "damaged" sections*
Outer dimension of hollow cross-section	0.05 m	0.05 m
Tube thickness	2.16 mm	1.65 mm
Cross-sectional area	410.57 mm^2	324.57 mm^2
Moment of inertia	162,526 mm^4	130,811 mm^4

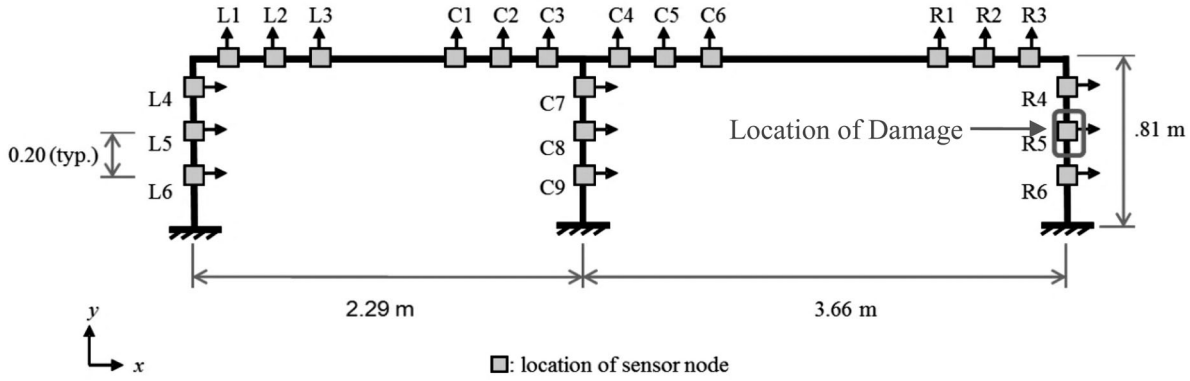

Fig. 2. Sketch of the specimen and the location of the introduced damage.

frequencies are much lower than the sampling rate as not to cause aliasing in the data. Because the data used in this study was collected from the real testbed structure, it already contains measurement noise as opposed to the simulation results in which artificial simulated noise is often added to the signal. Note that the effect of higher noise levels in the measurement on the performance of IDDA is studied previously and can be found in Dorvash et al. (2013). Results from these tests are shown in Section 5.

4.2 Loading scenarios for implementation of damage detection algorithm

A realistic scenario for implementation of the damage detection algorithm on real-life structures is to collect the ambient response of the structure before and after damage. The algorithm introduced is only suitable for a linear damage defined by Doebling et al. (1998) as "the case when the initially linear–elastic structure remains linear–elastic after damage." Thus, it is acceptable to assume that the behavior of the structure is within the linear elastic range in which small angle theory applies (Dorvash et al., 2013). Hence, in this implementation of the damage detection algorithm on the laboratory specimen, the excitation amplitude of the laboratory specimen was limited not to contradict this assumption.

Additionally, to consider the dynamic effects in the frame response two removable lumped masses (lifting weights) are attached to the frame at the middle of the spans. The weights are selected in the possible range of live loads to which such a frame would be subjected.

It should be noted that the addition of the mass to the frame is limited to the tests where multivariate methods are applied. This is because a univariate method is not proper for modeling the system with dynamic effects. Pakzad (2008) and Chang (2010) have presented simulated examples that support this assumption reasoning that if the stiffness of a structure is much larger than the mass, then the influence of the mass term becomes negligible and the dynamic equation of motion can be reduced to a static one. This is only valid, however, within a local joint where nodes are close to each other. Therefore, this article only creates damage features for nodes that are within the same local joint of the experimental structure.

To take the dynamic effects into consideration, impact load is chosen as a means of excitation. Thus, the excitation does not have frequency content of any particular range. It should be noted that other forms of excitation can be used with this algorithm. This is shown in Dorvash et al. (2010) in which simulations are used to prove that theoretically, in a stiff system with small mass, IDDA should detect damage regardless of excitation type. To apply impact load, the frame is tapped with a light hammer on the beam–column connection at the right side of the frame. The time history raw data of sensor L4 before and after damage is shown in Figure 3.

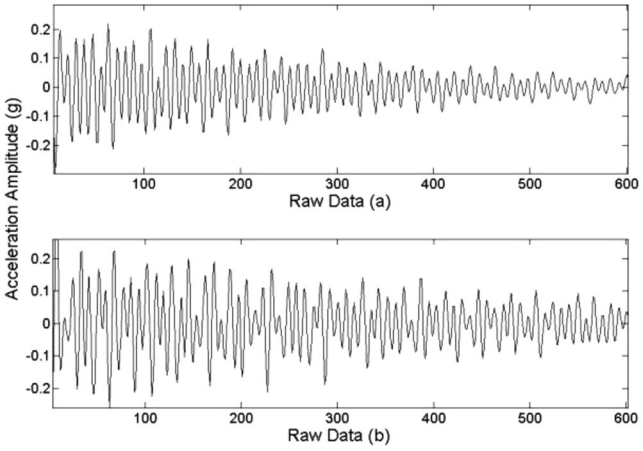

Fig. 3. Sample time history data from sensor L4 (a) before and (b) after the damaging event.

4.3 Implementation of the damage detection on the test frame

4.3.1 Univariate regression. Univariate regression, based on Equation (11) is used to find the influence coefficients α. To verify the accuracy of the estimated coefficient, *Evaluation Accuracy* (EA) and *Estimation Error* (γ) parameters are used. These parameters ensure that the influence coefficients are correctly reflecting the properties of the frame.

EA_{ij} is defined as the product of influence coefficients α_{ij} and α_{ji} as

$$EA_{ij} = \alpha_{ij}\alpha_{ji} \tag{12}$$

A value for their product close to unity signifies a strong accuracy of estimation and a product of less than unity corresponds to progressively higher values of the noise and nonlinear behavior of the physical structure. The normalized estimation error, γ_{ij}, can be calculated by

$$\gamma_{ij} = \frac{\sigma_{\alpha_{ij}}}{\alpha_{ij}} \tag{13}$$

As noted above, α_{ij} is the influence coefficient between nodes i and j, and is the standard error of the influence coefficient estimates. Note that, σ_{aij} is estimated by Equation (14)

$$\sigma_{\alpha_{ij}} = \frac{\sigma_e}{(\sum y_i^2)^{1/2}} \tag{14}$$

Here, σ_e is the standard error of the estimation residuals (i.e., the standard deviation of the vector obtained by subtraction of the estimated response from the true response) and y_i is the response at node i which is regressed with respect to the response at node j (y_j). Considering that the response has a zero mean, the denominator of Equation (14) is simply the standard deviation of the response at node i. This equation is utilized to show that a low standard deviation of the influence coefficients, which corresponds to a more accurate estimate, produces a low estimation error. Hence, the closer the γ_{ij} is to zero, the less error is associated with the estimated damage indicator α_{ij}. Figures 4a and b show typical univariate linear regression coefficients and their corresponding Evaluation Accuracy and Estimation Error parameters for the influence coefficient α_{ij} in Equation (11), for locations 5 and 6, namely α_{56}, for both, the left side (shortened to $\alpha_{56\text{-L}}$) and the right side ($\alpha_{56\text{-R}}$) of the frame. This coefficient will be used as an example plot for all three univaraite control statistics being investigated.

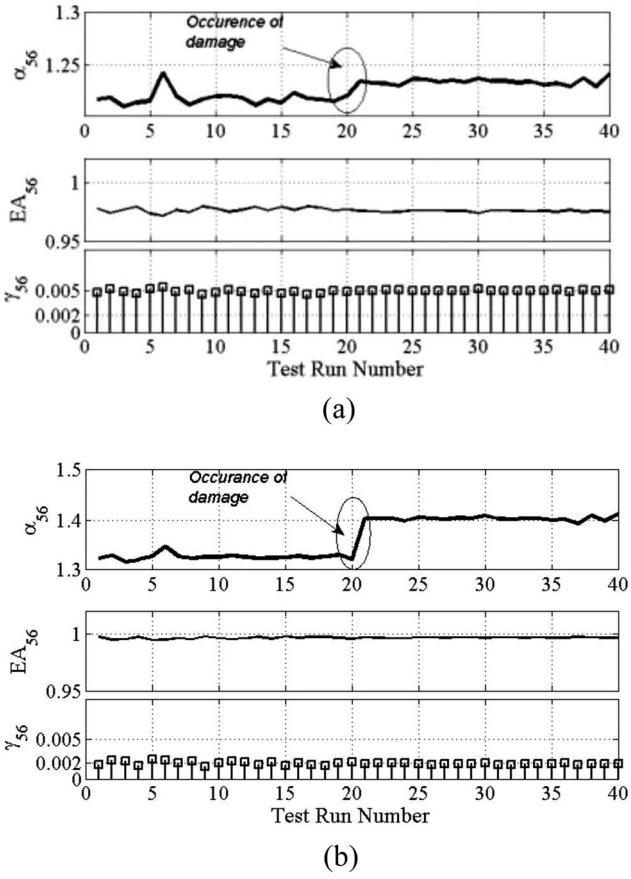

Fig. 4. Results for the coefficient values, accuracy and error parameters for (a) coefficient $\alpha_{56\text{-L}}$ and (b) coefficient $\alpha_{56\text{-R}}$.

It is crucial to use a damage feature that changes with the properties of the structure. Even though the timing of damage would be unknown, a comparison between the undamaged and damaged features was generated to evaluate the effectiveness of these damage features. If no difference is found between a location

near and far from damage, these features would be deemed less effective in identifying the location of damage. The first graph in each plot in Figure 4 shows the magnitude of the coefficient for all 40 runs. For the left side coefficient, $\alpha_{56\text{-L}}$ shown in Figure 4a, the mean of the first 20 (undamaged) runs is different from that of the last 20 (damaged) runs by 1.25%. On the right side ($\alpha_{56\text{-R}}$), however, this variation increases to 5.50% as shown in Figure 4b. This indicates that the right side properties of the frame have changed more than the left side. In using a control chart, the timing and location of the damage should be indicated because these parameters are previously unknown in real damage detection scenarios. Note that the accuracy parameter does not deviate far from one on both of these graphs which indicates that these parameters should not be disregarded as false alarms. Additionally, the Estimation Error can be used to further justify these coefficients as correct representations of the properties of the frame.

4.3.2 Multivariate model. This section presents the application of multivariate damage feature techniques for deployment of higher order models. To use the Mahalanobis distance and the Fisher Criterion to detect changes in the state of the structure, a multivariate autoregressive model is utilized.

An important aspect of ARX modeling is choosing the model order that well suits the data but also does not cause over-parameterization (Figueiredo et al., 2011). One way to establish the model order (P and Q in Equation (10)) is to minimize the Akaike's Information Criterion (AIC) which is defined as,

$$\mathrm{AIC}(k) = -2\log L\left(\hat{\theta}_k\right) + 2k \tag{15}$$

In Equation (15), k is the number of parameters in the statistical model and $\hat{\theta}_k$ is the maximized value of the likelihood function. The AIC provides two objectives: it rewards goodness of fit, but also discourages overfitting so that the model order does not become too large (Bozdogan, 1987).

The AIC is calculated for the test consisting of impact excitation to the frame with added mass. The AIC indicator has its lowest value for model order two for most runs and sensor locations. As a result, the multivariate change point analysis methods used in this study will set P and Q in Equation (10) to two for the data collected from tests with mass added to the system. In a similar manner, the model order of data without added mass was found to be four. For simplicity, the order of P and Q are kept the same.

5 RESULTS AND COMPARISON

Because the damage case being considered is a section on the right side column, the results for each method should detect damage at or near this location. Only the results on the left and right side of the frame are compared and presented for simplification. There are six sensors on each side of the frame resulting in 30 pairs of different nodes. First, the statistical methods are examined to see if they correctly identify occurrence of the change point at the 21st run, when the damage is introduced. Then, it is further inspected to determine if it can provide where damage occurred.

5.1 Estimated weighted moving average for univariate model

The process is considered out of control when the Z value in Equation (1) falls outside the range of the control limits. As stated previously, the conventional threshold from Lucas and Saccucci (1990) is three standard deviations away from the mean. However, when this method is implemented, damage was not detected anywhere on the frame as plots from both the left and right side of the frame never crossed the boundaries. As a result, this way of determining thresholds is deemed insufficient. It is reasonable to decrease the value of L for it corresponds to a 99.7% confidence, creating a very large confidence region. However, a bootstrap is used to compare the effectiveness of some of the EWMA statistic to other univariate methods in this article. The results of the EWMA bootstrapped plot of α_{56} are shown in Figures 5a and b, respectively.

It is important to note that there is a well-defined change in the EWMA slope for the original data at the 21st run, as soon as the damage cases are included in the statistic. Once the threshold is crossed, the change can be considered assignable and it can be concluded that the frame was damaged near this location. In Figure 5a, the left side coefficient $\alpha_{56\text{-L}}$ does not cross the bounds created by the bootstrap. This indicates that the frame's properties do not change significantly near these sensors. However, in Figure 5b the EWMA for $\alpha_{56\text{-R}}$ does cross the threshold; therefore, the properties of the right side of the frame near sensor locations R5 and R6 do change significantly with a 91% confidence level using Equation (7). These results are consistent with the damage case. Every sensor pairing plot is analyzed in a similar fashion and the results confirm that there is damage on the right side column of the frame. Additionally, the EWMA plot crosses the bounds at the 25th run which is a delayed, but quick detection of a change in the system. Because the change being detected is a step change, it may take a few data sets from the damaged

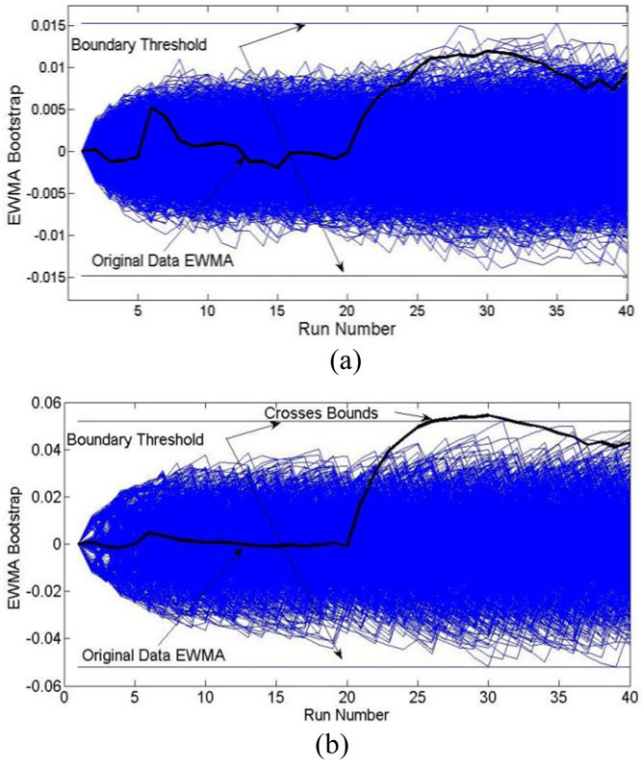

Fig. 5. Typical plots for the Exponentially Weighted Moving Average (EWMA) with bootstrapping for the (a) coefficient $\alpha_{56\text{-L}}$ and (b) coefficient $\alpha_{56\text{-R}}$.

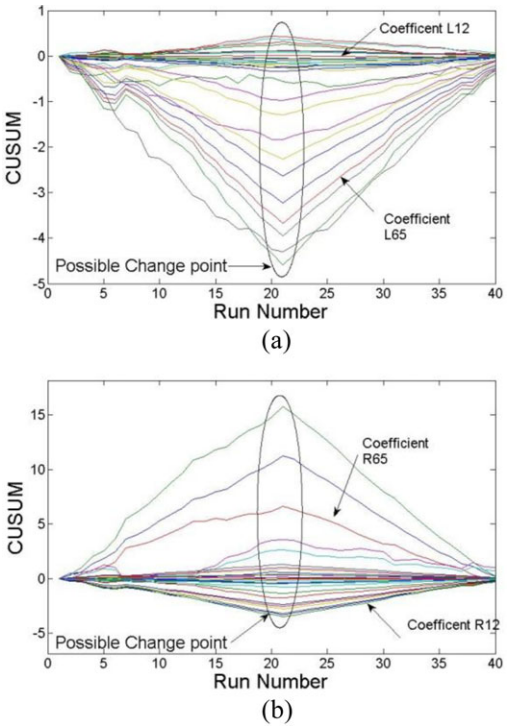

Fig. 6. Cumulative Sum (CUSUM) charts for (a) the left and (b) right side of the frame. Shows no boundary for detecting damage, just a possible change point.

structure for it to mark its effect on the statistic. Therefore, the change is not detected until five damaged runs are included in the EWMA. Still, it correctly identifies the correct time and location of damage.

5.2 CUSUM chart for univariate coefficients

The CUSUM plots that were created for the left and right side of the specimen are shown in Figures 6a and b, respectively. Both plots exhibit a change in slope at the 20th run thus indicating a possible change point at the 21st run. Therefore, the CUSUM correctly identifies when the change occurred; however, this does not help differentiate the left side from the right side and thus does not provide a location of damage.

Because the entire structure's response is affected by the damaged section, the left side CUSUM shows a change in slope as well. However, the change should not be as significant on the left as on the right side considering the damage case in question. It is noted that in Figure 6, the ranges of the CUSUM are a lot smaller for those sensor locations on the left side of the frame which would indicate that the properties of the structure on the right side have changed more compared to the left side. Yet, no conclusion can be made about the significance of the change.

To create the necessary threshold bound, bootstrapping is used to show if the change of properties on the right side of the frame is indeed significant. The left side CUSUM charts should remain within the range of bootstraps; yet, the CUSUM charts for the right side coefficients should cross the bounds of the bootstrap as close to the 21st run as possible at locations near damage. The α_{56} bootstrapped plots for $\alpha_{56\text{-L}}$ and $\alpha_{56\text{-R}}$ are shown in Figures 7a and b for the left and right sides, respectively.

In Figure 7 the CUSUM chart for coefficient $\alpha_{56\text{-R}}$ crosses the confidence bound produced by the bootstrap. Using Equation (7), this indicates damage is detected at this sensor pairing with a 98.8% confidence level. Additionally, this method detects damage at the 21st run, which is a very quick detection scheme. On the other hand, the bootstrap threshold is not exceeded for coefficient $\alpha_{56\text{-L}}$, indicating no damage at this location. Charts are created for all sensor pairings on the frame and it is very evident that there is a significant change on the right column of the frame.

It should be noted that those locations closest to damage are also susceptible to change and cross a threshold for an in control process. With the use of a dense sensor network, these changes can be detected. For

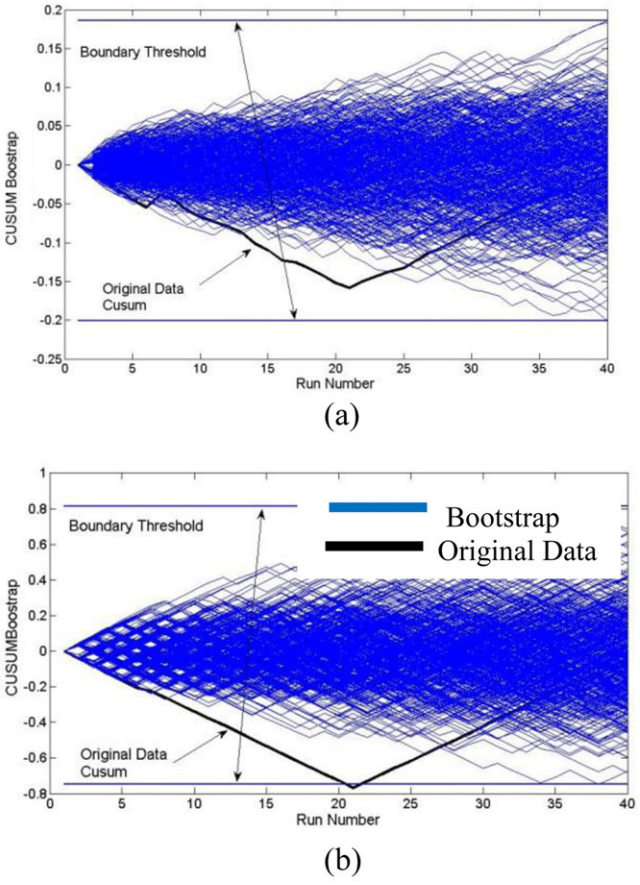

Fig. 7. Typical plots for the Cumulative Sum (CUSUM) with bootstrapping for (a) coefficient $\alpha_{56\text{-L}}$ and (b) coefficient $\alpha_{56\text{-R}}$.

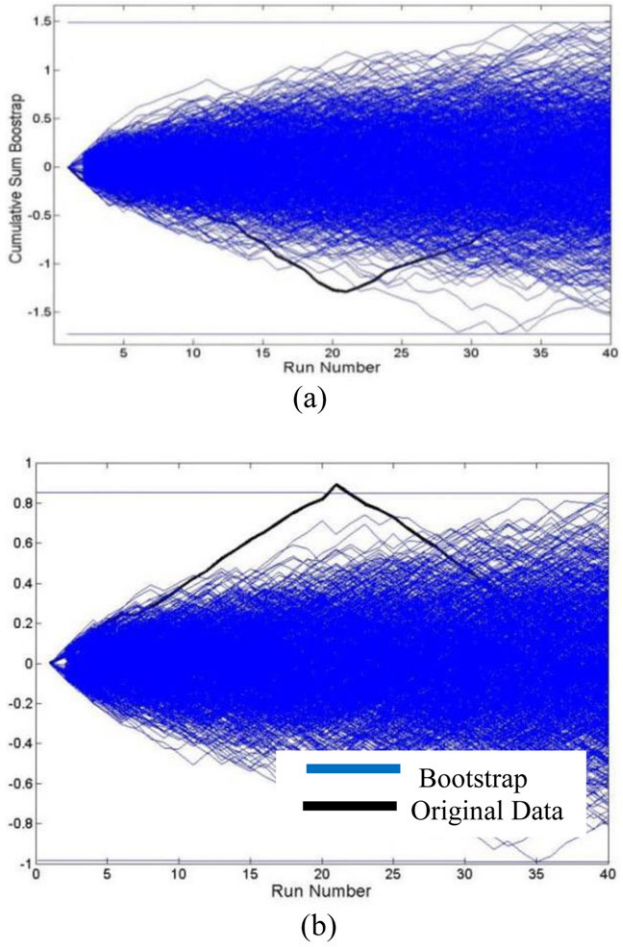

Fig. 8. Typical Cumulative Sum plots for coefficient (a) $\alpha_{56\text{-L}}$ and (b) coefficient $\alpha_{56\text{-R}}$.

example, Figure 8 is a CUSUM with bootstrapping for the univariate influence coefficient α_{46} on both the left and right sides. This coefficient involves the two closest locations to the actual damage (R4 and R6). It is shown here that damage is indicated at these locations on the right side of the frame but not the left.

The results show damage at sensor locations R4 and R6. These locations are not directly at the damage, but because of their proximity to sensor R5, they show a more significant change than others. Conversely, the left side CUSUM plots have a range very similar to the bootstraps. Because the bootstraps are supposed to simulate data that has no damage, the left side of the frame can be characterized as so. In effect, the CUSUM correctly identifies the occurrence and location of damage.

5.3 MSE for univariate model

The MSE algorithm separates the coefficients from all 40 runs into two segments and finds the MSE associated to each segment. An example of the results is shown in Figures 9a and b where the MSE indicator is plotted for all 30 coefficients on the left and right side of the frame respectively. The 20th run marks the lowest value for the MSE implicating the 21st run as the first possible index of the damaged state.

This is the correct timing of damage; however, this plot, like the CUSUM chart, does not allow the observer to detect the location of damage. As a result, a bootstrap was generated to establish a threshold and the results are shown in Figures 10a and b for coefficient $\alpha_{56\text{-L}}$ and $\alpha_{56\text{-R}}$, respectively. It is expected, as shown in the CUSUM and EWMA plots previously, that the $\alpha_{56\text{-R}}$ coefficient crosses the $\alpha_{56\text{-R}}$ bounds near the 21st run and the $\alpha_{56\text{-L}}$ coefficient does not cross at all.

However, the MSE plot of this sensor pairing crosses the bounds on both plots shown in Figure 10. This implies that both $\alpha_{56\text{-L}}$ and $\alpha_{56\text{-R}}$ undergo a significant change in the data and therefore signify a damaged

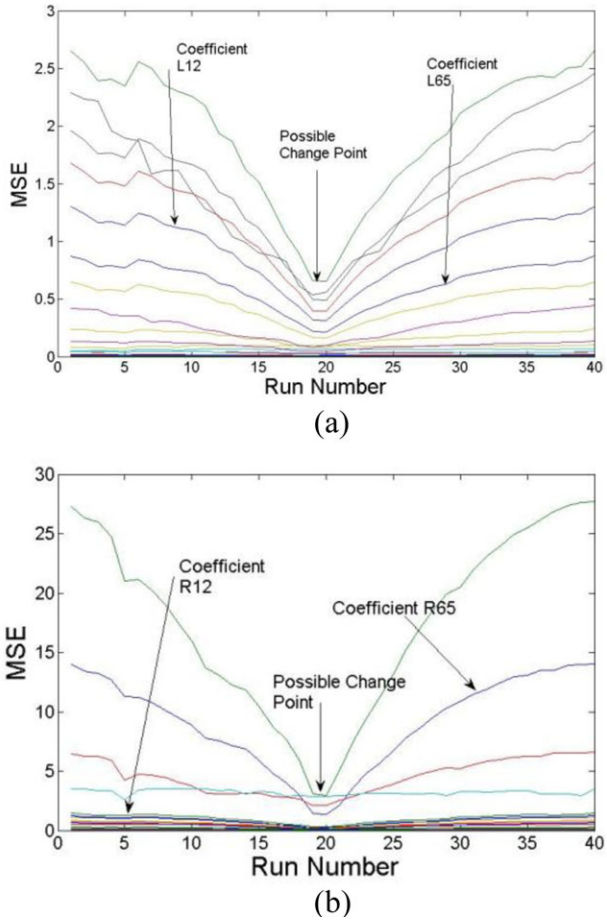

Fig. 9. Plots of Mean Square Error (MSE) Indicator for (a) coefficient $\alpha_{56\text{-L}}$ and (b) coefficient $\alpha_{56\text{-R}}$. Similar to the CUSUM chart, it does not show a location of damage on its own.

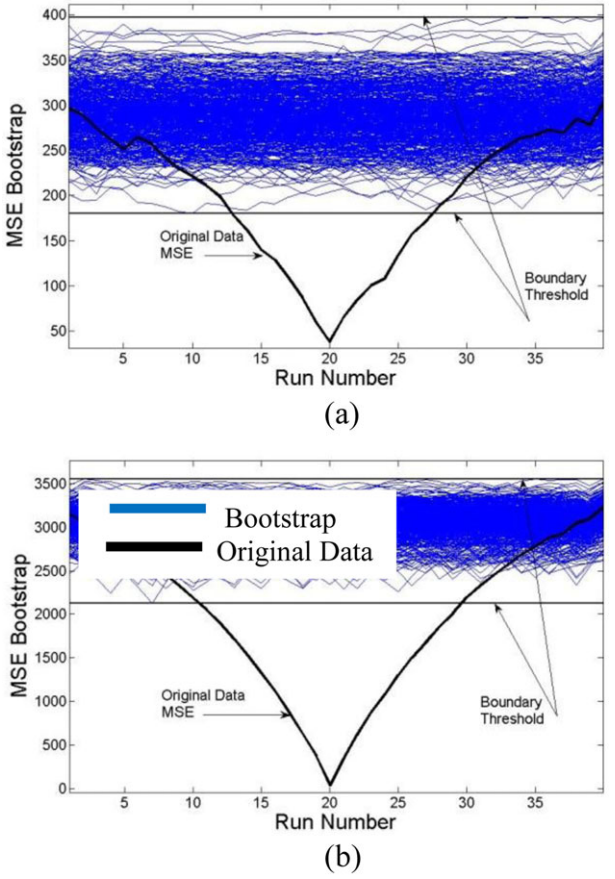

Fig. 10. Typical Mean Square Error (MSE) plots for (a) coefficient $\alpha_{56\text{-L}}$ and (b) coefficient $\alpha_{56\text{-R}}$. The threshold limit is crossed within the supposed undamaged runs and the bootstrap does not fit the data.

section. Additionally, the MSE plot crosses the bound around the 13th run which is well before the damage occurs. Hence, both the timing and placement of damage from these plots are misleading and the statistic must be changed to detect the correct location and time of damage. As stated earlier, damage detection using control charts relies on the change in the mean and constant variance. Therefore, the ModMSE can be used, shown in Equation (6), which expunges the variance between the two segments produced and maintains their independent means.

Before a bootstrap is conducted, the difference between the original MSE and the ModMSE is inspected using a similar approach to the CUSUM indicator discussed in Section 2.1. Because the MSE may not start or end at zero, the ranges of the statistic were recorded instead of the largest magnitude. On the plots in Figures 11a and b, the ranges of the MSE and ModMSE, respectively, are shown for all 60 coefficients. The first 30 coefficients are from the left side and last 30 coefficients are from the right side. Additionally, a boundary condition of three standard deviations away from the mean (a normal procedure of a Shewhart control chart from Lucas and Saccuci, 1990) is used for a simple comparison.

Figure 11a shows the MSE range plot using the original MSE coefficients. This model detects damage at sensor locations R1, R2, R3, and R4 which are located on the right beam and column close to the joint. Although these locations are on the right side of the frame, the actual location of damage, R5, is not included or detected. On the other hand, the normalized MSE statistic, ModMSE, was then used to create the same plot and the results are shown in Figure 11b where the damage is correctly identified. Sensors R3, R4, and R6, along with R5, show a significant change in properties because of their proximity to the damage; hence, the ModMSE shows spikes for the coefficients $\alpha_{54\text{-R}}$, $\alpha_{43\text{-R}}$, $\alpha_{36\text{-R}}$, and $\alpha_{61\text{-R}}$.

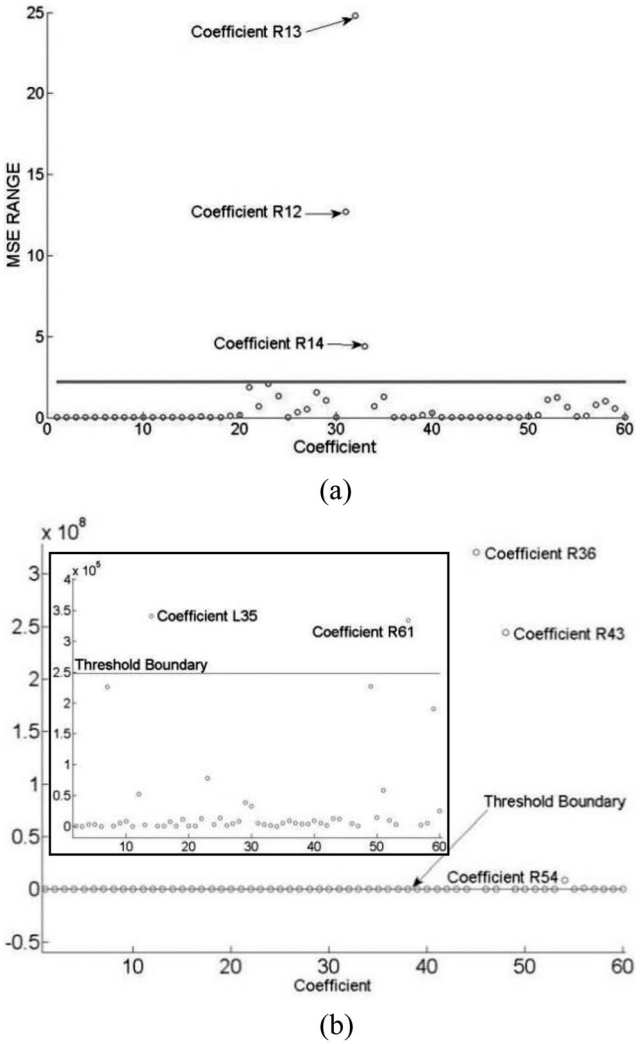

Fig. 11. The magnitudes of the (a) Mean Square Error (MSE) and (b) ModMSE for all pairs of coefficients.

Additionally, false alarms can be eliminated by using the Evaluation Accuracy and Estimation Error parameters. To rely on influence coefficient changes as indicator of damages, the Evaluation Accuracy should be close to unity (e.g., greater than 0.95) and the Estimation Error should be close to zero (e.g., less than 0.05). If these numbers are low and high respectively, the coefficient should be disregarded because it is not correctly representing the properties of the frame in accordance with the assumptions made.

As shown in Figure 11b, coefficient $\alpha_{35\text{-L}}$ seems to cross the bounds, signifying a damage location. However, it is at this point that the accuracy and error parameters associated with the sensor pairing, shown in Figure 12, can be used to eliminate it as a false alarm. The accuracy and error parameters are very high and

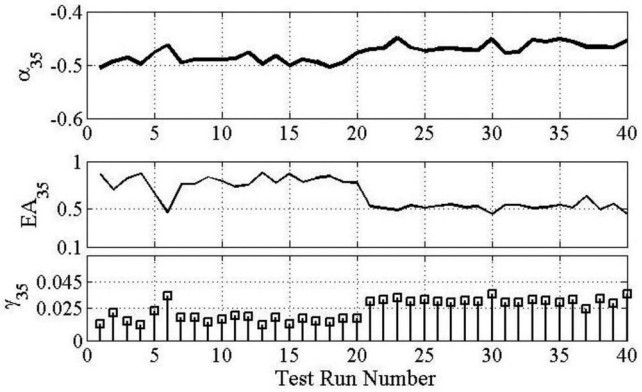

Fig. 12. Eliminating false alarms: the accuracy and error parameters associated with coefficient $\alpha_{35\text{-L}}$ can be analyzed to correct for any false results.

low respectively; hence, this coefficient can be disregarded.

Now that the ModMSE has shown the correct location of damage in Figure 11, a bootstrap can be generated to analyze its results to compare it to the EWMA and CUSUM plots previously discussed. The results of the bootstrap are shown in Figures 13a and b for the left, $\alpha_{56\text{-L}}$ and right, $\alpha_{56\text{-R}}$ coefficient, respectively.

In using the ModMSE, damage is correctly detected at sensor pairing $\alpha_{56\text{-}R}$ because the right side coefficient crosses the bound at the 21st run (i.e., as soon as the damage occurs).

Additionally, the left side coefficient $\alpha_{56\text{-L}}$ does not cross the boundary, indicating an undamaged location. This demonstrates that the ModMSE, like the already established indicators CUSUM and EWMA, can be used to correctly find the timing and location of damage.

5.4 Multivariate Mahalanobis distance

Histograms are used as a means to plot the Mahalanobis distances because coefficients with the largest distance are those that are closest to a location of damage and stay furthest from the baseline state. First, Mahalanobis distances are calculated between coefficients from the first 10 healthy state runs and the last 10 healthy state runs. This step creates a baseline distance. Then, the first 10 healthy runs and the 20 damaged runs are used to create a distance to compare to the reference. The distances calculated in the latter coefficients should be bigger than the baseline condition at areas of damage. As discussed in Section 4.2, two testing conditions are used for the multivariate data: a system with added mass and a system without mass. The two sets of results

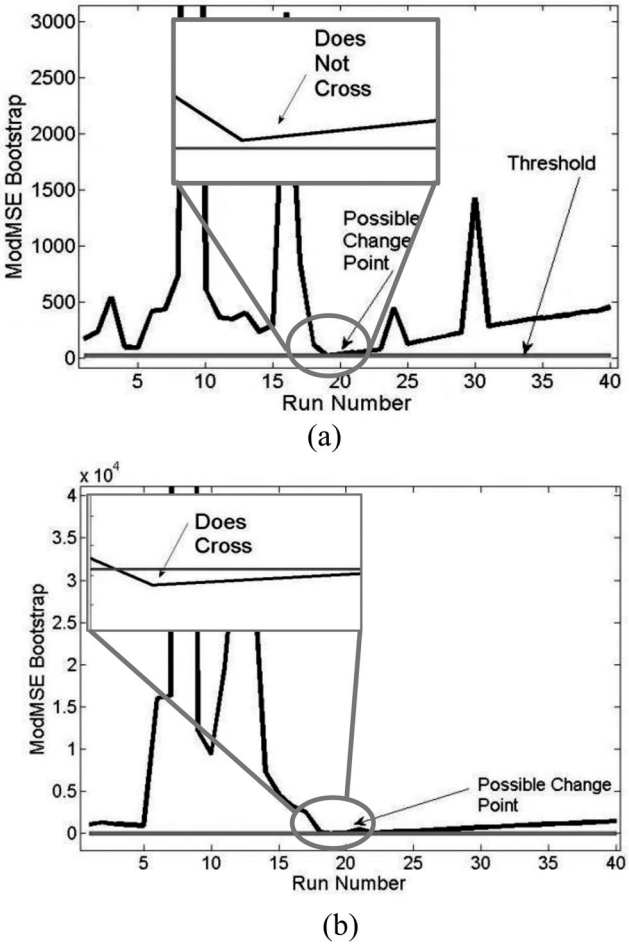

Fig. 13. Modified Mean Square Error (ModMSE) Bootstrap for (a) coefficient $\alpha_{56\text{-L}}$ and (b) coefficient $\alpha_{56\text{-R}}$.

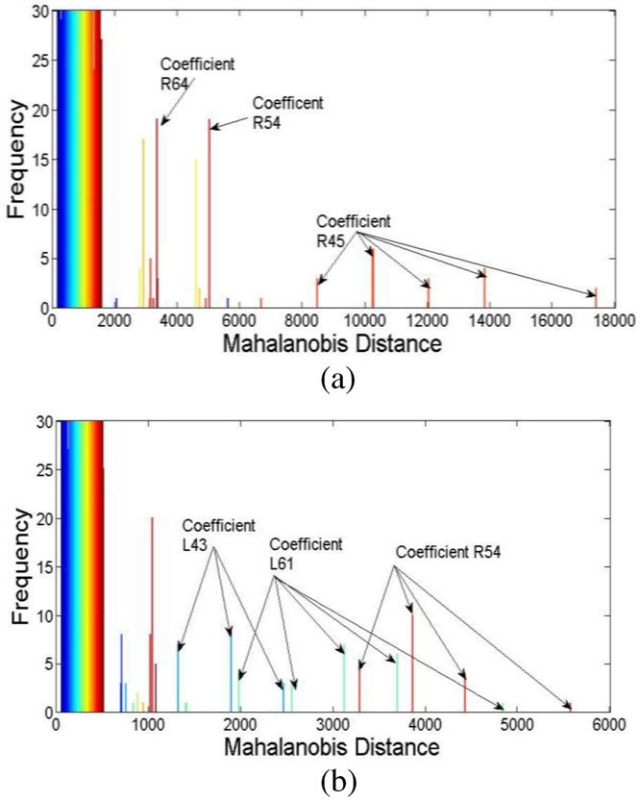

Fig. 14. Mahalanobis distance histograms for data (a) with mass and (b) without mass.

obtained from these two testing conditions are shown in Figures 14a and b.

To analyze these results, the sensor pairings with the larger Mahalanobis distances are deemed closer to a possible damaged location because they deviate more from the reference condition. Using the impact test data with added mass, shown in Figure 14a, the Mahalanobis distances have the greatest magnitude for coefficients $\alpha_{45\text{-R}}$, $\alpha_{54\text{-R}}$, and $\alpha_{64\text{-R}}$. Overall coefficient $\alpha_{45\text{-R}}$ has the greatest distance and this result properly indicates the location of damage. Yet, the results from the test data without mass, in Figure 14b, show to be inconsistent. Sensors from the left side of the frame, $\alpha_{43\text{-L}}$ and $\alpha_{61\text{-L}}$, as well as sensor pairing $\alpha_{56\text{-R}}$ have large Mahalanobis distances; despite these observations, without a threshold, it cannot be concluded that any location is necessarily undamaged or damaged. Hence, the next section introduces the Fisher Criterion to minimize the discrepancy of damage localization by creating a threshold boundary.

5.5 Multivariate Fisher Criterion

The Fisher Criterion is used to create the boundary threshold for the Mahalanobis histogram that is necessary to distinguish the location of damage and the state of the structure. Figures 15a and b, show the Fisher Criterion for the impact tests with and without added mass, respectively. This statistic, as explained in Section 2.2, statistically determines the significance of the deviation of the larger distances from the baseline.

When the Fisher Criterion is analyzed using the tests with mass added to the system, the results correctly point to the location of damage. The coefficients that cross the threshold indicating damage are at $\alpha_{43\text{-R}}$, $\alpha_{53\text{-R}}$, and $\alpha_{63\text{-R}}$. Although there is no damage associated with sensors R4, R6, and R3, these locations are the closest to sensor R5 where the damage is located. It is reasonable that the coefficients corresponding to these sensor pairings also cross a damaged boundary.

Similarly, the Fisher Criterion results for tests without added mass show the correct location of damage

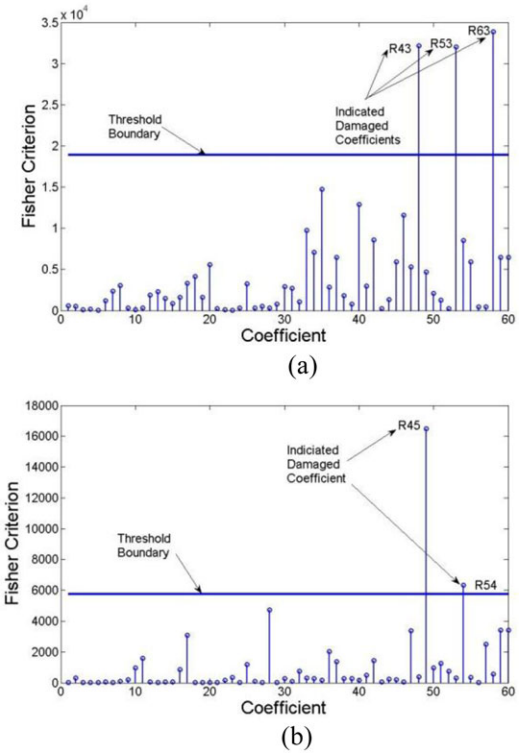

Fig. 15. Fisher Criterion plots for data (a) with mass and (b) without mass.

while also eliminating the discrepancies from the Mahalanobis distance results. The only sensor coefficients that cross the bounds are $\alpha_{45\text{-R}}$ and $\alpha_{54\text{-R}}$ corresponding to sensor pairings that are located on the right side column of the frame. Although the histogram in Figure 14b shows large values for coefficients $\alpha_{43\text{-L}}$ and $\alpha_{61\text{-L}}$ for the impact data without added mass, the Fisher Criterion plot eliminates these as false alarms of damage detection because these values remain well below the threshold. These results indicate that the Mahalanobis distance statistic can be used in conjugation with the Fisher Criterion to properly indicate the location of damage. It can be noted that the timing of a possible damaging event is assumed to be known; the distances are calculated using the two separate sets of data from pre and post damaging event.

5.6 Summary of methods

To provide a summary on the characteristics of all the discussed change point detection methods, Table 2 is presented which includes all methods, along with a summary of each.

Table 2
Summary review of change point detection methods

Method	*Comments*
Exponentially Weighted Moving Average	Simplified threshold of three standard deviations away from the mean cannot be used; however, bootstraps can be used as a threshold generator
Cumulative Sum	Good for many different types of data sets; however, too simple, may not be sensitive to smaller shift changes or drifts changes
Mean Square Error	Sensitive to variation in data set; hence ModMSE was introduced
ModMSE	Eliminates the sensitivity of the MSE statistic to the change in variance of the data
Mahalanobis distance	Very efficient in condensing a set of damage features; however, no clear threshold value using histogram alone
Fisher Criterion	Uses a simple threshold of 1.96 standard deviations away from the mean; in effect it eliminates discretion of Mahalanobis distance histogram

6 CONCLUSIONS

Change point analysis is essential in detecting damage in a structure. There are many factors (e.g., variation in environmental and operational condition) that can contribute to a change in structure's response and thus in damage indices of a damage detection algorithm. Therefore, statistical frameworks can be used to distinguish between common and assignable changes by creating boundary limits for changes in a process (i.e., variation of damage indices). There are many change point detection methods that are used in various industries. However, for their implementation in SHM schemes, the statistic and/or boundary limit generation may need adaptations. In this article, several change point detection algorithms are examined, and an improved algorithm for the MSE is developed and presented. This statistic is used to monitor the change in the mean of a data set and if the variance in the data set is too large, it may mask the change in mean. Therefore, the modified ModMSE is introduced, which expunges the variance of the data set, and its application and effectiveness are demonstrated in this article. Additionally, it is shown that the simplified predetermined control limit for the EWMA is a very simple, although sometimes ineffective way of determining a boundary and may not work for all data types. Moreover, it is subject to the

distribution of the data because it is based on a normal distribution assumption.

Furthermore, the threshold generating methods described in the article can be used for unknown damage because they are statistically generated to produce a boundary for an in control process. However, they can be manipulated (e.g., through change in number of bootstraps) for user defined confidence levels which makes them suspect to inconsistencies. Therefore, it is recommended that for civil engineering damage detection purposes, in using univariate and/or multivariate control charts, a "shotgun approach" be utilized in which multiple charts be used on the same data set to coordinate damage localization.

Through implementation of IDDA on a laboratory model, it is shown that IDDA, when combined with the control charts, is an effective and efficient damage detection scheme. The implementation of change point detection methods with IDDA features, presented in this article accurately locates the damage using statistically generated threshold values to determine the significance of change. Yet, with an increase in the amount of output channels, the accuracy and resolution of the detection of change can increase without a loss for efficiency in time for computation. Moreover, considering the recent technological advancements in sensing technology, affordable sensors (such as wireless sensors) can address the need for the high number of outputs (sensors) without significant economic burden. However, the location and number of sensors can have an effect on the accuracy and resolution of damage detection. Study of such effects will be considered in future work.

ACKNOWLEDGMENTS

Research funding is partially provided by the National Science Foundation through Grant No. CMMI-0926898 by the Sensors and Sensing Systems Program, and by a grant from the Commonwealth of Pennsylvania, Department of Community and Economic Development, through the Pennsylvania Infrastructure Technology Alliance (PITA). This financial support is gratefully acknowledged.

REFERENCES

Adeli, H. & Jiang, X. (2009), *Intelligent Infrastructure—Neural Networks, Wavelets, and Chaos Theory for Intelligent Transportation Systems and Smart Structures*, CRC Press, Taylor & Francis, Boca Raton, FL.

Alvandi, A. & Cremona, C. (2006), Assessment of vibration-based damage, *Journal of Sound and Vibration*, **292**, 179–202.

Bozdogan, H. (1987), Model selection and Akaike's information criterion (AIC): the general theory and its analytical extensions, *Psychometrika*, **52**(3), 345–70.

Chang, M. (2010), Damage detection and modal identification of structural systems using sensor data. M.S. thesis, Lehigh University, Bethlehem, PA.

Cruz, P. J. S. & Salgado, R. (2009), Performance of vibration-based damage detection methods in bridges, *Computer-Aided Civil and Infrastructure Engineering*, **24**(1), 62–79.

Doebling, S. W., Farrar, C. R. & Prime, M. B. (1998), A summary review of vibration-based damage identification methods. *Shock and Vibration Digest*, **30**(2), 91–105.

Dorvash, S. Pakzad, S. N. & and Labuz, E. (2013). Statistics based localized damage detection using vibration response, (IOP publishing) smart structures and systems, *An International Journal*. In Press.

Dorvash, S., Pakzad, S. N., Labuz, E., Chang, M., Li, X. & Cheng, L. (2010), Validation of a wireless sensor network using local damage detection algorithm for beam-column connections, in *Proceedings of the SPIE*, **7647**, DOI:10.1117/12.847581.

Farrar, C. R., Baker, W. E., Bell, T. M., Cone, K. M., Darling, T. W., Duffey, T. A., Eklund, A. & Migliori, A. (1994), *Dynamic Characterization and Damage Detection in the I-40 Bridge Over the Rio Grande*, Los Alamos National Laboratory Report LA-12767-MS.

Farrar, C. R., Duffey, T. A., Doebling, S. W. & Nix, D. A. (1999), A Statistical Pattern Recognition Paradigm for Vibration-Based Structural Health Monitoring, *Presented at the 2nd International Workshop on Structural Health Monitoring*. Stanford, CA.

Figueiredo, E., Figueiras, J., Park, G., Farrar, C. R. & Worden, K. (2011), Influence of the autoregressive model order on damage detection, *Computer-Aided Civil and Infrastructure Engineering*, **26**, 225–38.

Fugate, M. L., Sohn, H. & Farrar, C. R. (2001), Vibration-based damage detection using statistical process control, *Mechanical Systems and Signal Processing*, **15**, 707–21.

Glisic, B., Adriaenssens, S. & Szerzo, P. (2013), Structural analysis and validation of a smart pantograph mast concept, *Computer-Aided Civil and Infrastructure Engineering*, **28**(9), 651–65.

Gul, M. & Catbas, N. F. (2009), Statistical recognition for structural health monitoring using time series modeling: theory and experimental verifications, *Mechanical Systems and Signal Processing*, **23**, 2192–204.

Hampshire, T. A. & Adeli, H. (2000), Monitoring the behavior of steel structures using distributed optical fiber sensors, *Journal of Constructional Steel Research*, **53**(3), 267–81.

Hawkins, D. M. (1981), A CUSUM for a scale parameter, *Journal of Quality Technology*, **13**, 228–31.

Hotelling, H. (1947), Multivariate quality control illustrated by air testing of sample bombsights, in C. Eisenhart, M. W. Hastay, and W. A. Wallis (eds.), *Techniques of Statistical Analysis*, McGraw Hill, New York, pp. 111–84.

Hu, X. Y., Wang, B. & Ji, H. (2013), A wireless sensor network-based structural health monitoring system for highway bridges, *Computer-Aided Civil and Infrastructure Engineering*, **28**(3), 193–209.

Jiang, X. & Adeli, H. (2007), Pseudospectra, MUSIC, and dynamic wavelet neural network for damage detection of highrise buildings, *International Journal for Numerical Methods in Engineering*, **71**(5), 606–29.

Jiang, X. & Adeli, H. (2008a), Dynamic fuzzy wavelet neuroemulator for nonlinear control of irregular highrise building structures, *International Journal for Numerical Methods in Engineering*, **74**(7), 1045–66.

Jiang, X. & Adeli, H. (2008b), Neuro-genetic algorithm for nonlinear active control of highrise buildings, *International Journal for Numerical Methods in Engineering*, **75**(7), 770–86.

Khelifa, M. R. & Guessasma, S. (2013), New computational model based on finite element method to quantify damage evolution due to external sulfate attack on self-compacting concretes, *Computer-Aided Civil and Infrastructure Engineering*, **28**(4), 260–72.

Lucas, J. M. & Saccucci, M. S. (1990), Exponentially weighted moving average control schemes: properties and enhancements, American Statistical Association and the American Society for Quality, *Technometrics*, **32**(1), 1–12.

Luo, D., Ibrahim, Z, Xu, B. & Ismail Z. (2013), Optimization the geometries of biconical tapered fiber sensors for monitoring the early-age curing temperatures of concrete specimens, *Computer-Aided Civil and Infrastructure Engineering*, **28**(7), 531–41.

Macgregor, J. F. & Harris, T. J. (1990), Discussion of 'EWMA Control Schemes: properties and enhancement' by Lucas and Saccucci, American Statistical Association and the American Society for Quality, *Technometrics*, **32**(1), 1–29.

Mosavi, A. A., Dickey, D., Seracino, R. & Rizkalla, S. (2011), Identifying damage locations under ambient vibrations utilizing vector autoregressive models and Mahalanobis distances. *Mechanical Systems and Signal Processing*, **26**, 254–67.

Nichols, J. M., Trickey, S. T., Todd, M. D. & Virgin, L. N. (2003), Structural health monitoring through chaotic interrogation, *Meccanica*, **38**(2), 239–50.

Nishikawa, T., Fujino, Y., Yoshida, J. &Sugiyama, T. (2012), Concrete crack detection by multiple sequential image filtering, *Computer-Aided Civil and Infrastructure Engineering*, **27**(1), 29–47.

O'Byrne, M., Schoefs, F., Ghosh, B. & Pakrashi, V. (2013), Texture analysis based damage detection of ageing infrastructural elements, *Computer-Aided Civil and Infrastructure Engineering*, **28**(3), 162–77.

Osornio-Rios, R. A., Amezquita-Sanchez, J. P., Romero-Troncoso, R. J. & Garcia-Perez, A. (2012), MUSIC-neural network analysis for locating structural damage in truss-type structures by means of vibrations, *Computer-Aided Civil and Infrastructure Engineering*, **27**(9), 687–98.

Pakzad, S. N. (2008), Statistical approach to structural monitoring using scalable wireless sensor networks, Ph.D. dissertation, University of California, Berkeley.

Pandey A. K. & Biswas, M. (1995), Damage diagnosis of truss structures by estimation of flexibility change, *Modal Analysis – The International Journal of Analytical and Experimental Modal Analysis*, **10**(2), 104–17.

Park, H. S., Lee, H. M., Adeli, H. & Lee, I. (2007), A new approach for health monitoring of structures: terrestrial laser scanning, *Computer-Aided Civil and Infrastructure Engineering*, **22**(1), 19–30.

Philips, A. & Wu, Z. (2011), Vibration-based damage localization in flexural structures using normalized modal macrostrain techniques from limited measurements, *Computer-Aided Civil and Infrastructure Engineering*, **26**(3), 154–72.

Pompe, P. P. M. & Feelders, A. J. (1997), Using machine learning, neural networks, and statistics to predict corporate bankruptcy, *Computer-Aided Civil and Infrastructure Engineering*, **26**, 267–76.

Qioa, L. & Esmaeily, A. (2011), An overview of signal-based damage detection methods. *Applied Mechanics of Materials*, **94–96**, 834–51.

Qiao, L., Esmaeily, A. & Melhem, H. G. (2012), Signal pattern recognition for damage diagnosis in structures, *Computer-Aided Civil and Infrastructure Engineering*, **27**, 699–710.

Roberts, S. W. (1959), Control chart tests based on geometric moving averages, American statistical association and the American Society for Quality, *Technometrics*, **1**, 239–50.

Salawu, O. S. (1997), Detection of structural damage through changes in frequency: a review, *Engineering Structures*, **19**(9), 718–23.

Sirca Jr., G. F. & Adeli, H. (2012), System identification in structural engineering, *Scientia Iranica*, **19**(6), 1355–64.

Sohn, H., Czarnecki, J. A. & Farrar, C. R. (2000), Structural health monitoring using statistical process control, *Journal of Structural Engineering*, **126**(11), 1356–63.

Sohn, H., Farrar, C. R., Hunter, N. F. & Worden, K. (2001), Structural health monitoring using statistical pattern recognition techniques, *ASME Journal of Dynamics Systems, Measurement and Control*, **123**(4), 706–11.

Steiner, S. H. (1999), Exponentially weighted moving average control charts and time-varying control limits and fast initial response, *Journal of Quality Technology*, **31**, 75–86.

Tague, N. R. (2004), *The Quality Toolbox*, 2nd edn., pp. 155–8, ASQ Quality Press, Milwaukee, WI.

Talebinejad, I., Fischer, C. & Ansari, F. (2011), Numerical evaluation of vibration-based methods for damage assessment of cable-stayed bridges, *Computer-Aided Civil and Infrastructure Engineering*, **26**, 239–51.

Taylor, W. A. (2011), Change-point analysis: a powerful new tool for detecting changes. Available at: www.variation.com/cpa/tech/changepoint.html, accessed November 2013.

Umesha, P. K., Ravichandran, R. & Sivasubramanian K. (2009), Crack detection and quantification in beams using wavelets, *Computer-Aided Civil and Infrastructure Engineering*, **24**(8), 593–607.

Verdier, G. & Ferreira, A. (2011), Adaptive Mahalanobis distance and k-nearest neighbor rule for fault detection in semiconductor manufacturing, *IEEE Transactions on Semiconductor Manufacturing*, **24**(1), 59–68.

Walsh, S. B., Borello, D. J., Guldur, B. & Hajjar, J. F. (2013), Data processing of point clouds for object detection for structural engineering applications, *Computer-Aided Civil and Infrastructure Engineering*, **28**(7), 495–508.

Wang, Z. & Ong, K. C. G. (2008), Autoregressive coefficients based on Hotelling's T^2 control chart for structural health monitoring, *Computers and Structures*, **86**, 1918–35.

West, W. M. (1984), Illustration of the use of modal assurance criterion to detect structural changes in an orbiter test specimen, in *Proceedings of the Air Force Conference on Aircraft Structural Integrity*, pp. 1–6.

Xiang, J. & Liang, M. (2012), Wavelet-based detection of beam cracks using modal shape and frequency measurements, *Computer-Aided Civil and Infrastructure Engineering*, **27**, 439–54.

Xu, H. & Humar, J. (2006), Damage detection in a girder bridge by artificial neural network technique, *Computer-Aided Civil and Infrastructure Engineering*, **21**, 450–64.

Yao, R. & Pakzad, S. N. (2010), Autoregressive statisical pattern recognition algorithms for damage detection in civil structures, *Mechanical Systems and Signal Processing*, **31** (2012), 355–68.

Yao, R. & Pakzad, S. N. (2013), Time and frequency domain regression-based stiffness estimation and damage identification, *Structural Control and Health Monitoring* 10.1002/stc.1570.

Yin, T., Lam, H. F. & Chow, H. M. (2012), Bayesian probabilistic approach for crack characterization in plate structures, *Computer-Aided Civil and Infrastructure Engineering*, **25**, 375–86.

Zamba, K. D. & Hawkins, D. M. (2006), A multivariate change-point model for statistical process control, *Technometrics*, **48**(4), 539–49.